PHYSICAL REVIEW B **89**, 121106(R) (2014)

Temperature-dependent orbital physics in a spin-orbital-lattice-coupled $2p$ electron Mott system: The case of KO_2

Minjae Kim and B. I. Min
Department of Physics, PCTP, Pohang University of Science and Technology, Pohang 790-784, Korea
(Received 28 December 2013; published 13 March 2014)

We have investigated the temperature (T)-dependent evolution of orbital states in a typical spin-orbital-lattice-coupled $2p$ electron Mott system KO_2, based on the electronic structures obtained by the dynamical mean-field theory as well as the density functional theory. We have shown that KO_2 exhibits the orbital fluctuation feature at high T due to degenerate π_g^* orbitals. Upon cooling, the orbital fluctuation is suppressed by the Jahn-Teller-type crystal field that becomes stronger with the lowering of structural symmetry, and then the ferro-orbital (FO) ordering emerges at low T. This FO ordering feature distinguishes KO_2 from RbO_2 and CsO_2 in that the latter two seem to have antiferro-orbital orderings at low T, indicating that the underlying physics is different between them. We propose that the suppression of the orbital fluctuation in KO_2 can be observed by thermal-conductivity measurement, as observed in spin-orbital-lattice-coupled $3d$ transition-metal oxides such as $LaVO_3$.

DOI: 10.1103/PhysRevB.89.121106 PACS number(s): 75.47.Lx, 74.20.Pq, 75.25.Dk, 71.70.Ej

The spin-orbital-lattice coupling in transition-metal Mott insulators having degenerate d orbitals has been intensively investigated over the last decade [1–7]. According to their ground-state electronic structures, the degenerate d orbital systems can be classified into three categories. In the first category, the orbital degeneracy is lifted by the crystal field (CF), such as the Jahn-Teller (JT) effect and the hybridization with cations. The orbital polarization initially driven by the CF is stabilized further by the strong Coulomb correlation. Then the resultant orbital ordering determines the magnetic interaction. In the second category, the superexchange interaction of the Kugel-Khomskii (KK) type induces the orbital and magnetic orderings. Here the CF plays a secondary role in stabilizing the orbital ordering. In the third category, the orbital fluctuation exists in the degenerate orbitals, for which the relativistic spin-orbit coupling (SOC) becomes effective in determining the magnetic interaction.

It is interesting that the spin-orbital-lattice coupling exists also in $2p$ electron systems, such as AO_2 (A = Na, K, Rb, and Cs) alkali superoxides [8–16] and dioxygenyl O_2PtF_6 [17]. There are O_2^- anions in the former, while there are O_2^+ cations in the latter. As shown in Fig. 1, AO_2 consists of alkali A^+ cations and O_2^- molecule anions, and there are three electrons in the fourfold degenerate π_g^* orbitals. Hence, the orbital degeneracy occurs in a superoxide ion with 1 μ_B magnetic moment. According to the electron paramagnetic resonance (EPR) experiment, KO_2 has different crystal structures depending on temperature (T) [18,19]. For $T > 200$ K, it has the CaC_2-type tetragonal structure with the O_2 molecular axis along the z direction [T structure in Fig. 1(a)]. Upon cooling, the O_2 molecular axes in KO_2 rotate coherently. They rotate first around the [100] direction so as to have the rotation angle θ of 20° for $10 < T < 200$ K, which is denoted by the R[100] structure in Fig. 1(b). For $T < 10$ K, they rotate around the [110] direction to have $\theta = 30°$, denoted by the R[110] structure in Fig. 1(c) [20]. At this T, the antiferromagnetic (AFM) spin ordering emerges simultaneously [18–20]. In the AFM structure, the magnetic moments of O_2^- anions are ferromagnetically aligned in the (001) plane, while they are antiferromagnetically aligned along the c direction [23].

Distinct from KO_2, RbO_2 and CsO_2 have rather small rotation angles, $\theta < 5°$, in the whole T range. Namely, instead of the coherent rotation of O_2 molecular axes, the slight monoclinic and orthorhombic distortions occur for RbO_2 and CsO_2, respectively, upon cooling [14,18]. For RbO_2, the AFM structure has not been observed, while, for CsO_2, the one-dimensional (1D) AFM spin ordering, which is induced by the preexisting orbital ordering, has been observed [14].

There have been quite a few reports on the spin-orbital-lattice coupling in AO_2 superoxides [8–16]. Magnetic interactions in relation to crystal structure variation in KO_2 were discussed both experimentally [18,19] and theoretically [8]. Orbital states of KO_2 at high- and low-T crystal structures were also investigated by using the density functional theory (DFT) [10]. However, the investigation of the T-dependent evolution of electronic structures and orbital states in AO_2 in relation to the lowering of structural symmetry is still lacking.

In this Rapid Communication, we have explored T-dependent orbital states of KO_2 based on the electronic structures obtained by using the dynamical mean-field theory (DMFT) as well as the DFT. Orbital states of KO_2 at finite T are resolved in our study. We have demonstrated that the orbital fluctuation present at high T becomes completely suppressed upon cooling due to the lowering of structural symmetry. Then the AFM spin ordering occurs concomitantly with the emergence of the ferro-orbital (FO) ordering, which is driven by the CF of JT-type symmetry lowering. We have also shown that the situation in KO_2 is far different from those in RbO_2 and CsO_2, for which the CF due to the O_2 molecular axis rotation is not strong enough to induce the FO ordering.

For the DFT band-structure and total-energy calculations, we employed the full-potential augmented plane-wave band method implemented in the WIEN2k package [24,25]. We used the generalized gradient approximation (GGA) with incorporations of the SOC interaction and the on-site Coulomb interaction U of oxygen $2p$ electrons (DFT + U + SOC) [26]. We considered U values between 4 and 10 eV. We used 200 $\boldsymbol{k}$ points for the integration of the Brillouin zone [27]. We initialized the orbital density matrix to describe a specific orbital state. We used experimental lattice parameters $a = 4.030$ Å and $c = 6.697$ Å, and the bond length $d_{oo} = 1.306$ Å [19].

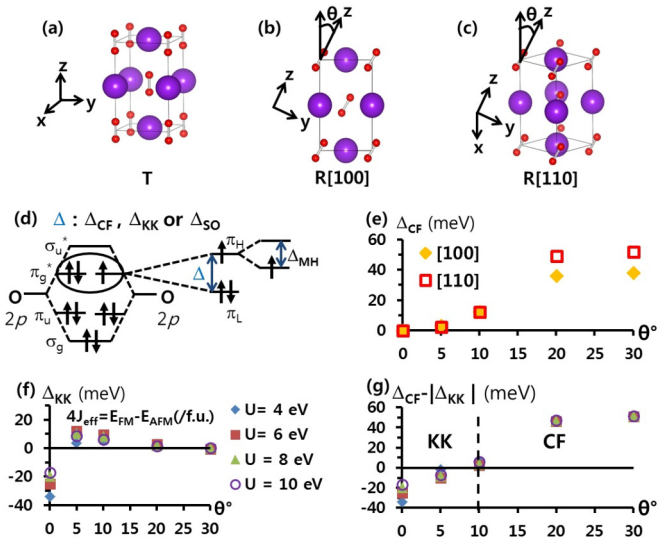

FIG. 1. (Color online) (a) Tetragonal (T) structure of KO_2, stable for $T > 200$ K. (b) R[100] structure of KO_2, stable for $10 < T < 200$ K, in which O_2 molecular axes rotate coherently around the [100] direction ($\theta \approx 20^\circ$). (c) R[110] structure of KO_2, for $T < 10$ K, in which O_2 molecular axes rotate coherently around the [110] direction ($\theta \approx 30^\circ$). This phase has simultaneous AFM and ferro-orbital (FO) orderings. (d) Schematic energy diagram showing electron occupation in a superoxide ion. Δ_{CF}, Δ_{KK}, Δ_{SO}, and Δ_{MH} represent the crystal field (CF) gap, Kugel-Khomskii (KK) gap, spin-orbit coupling (SOC) gap, and Mott-Hubbard gap, respectively. The magnitude of Δ_{SO} is ~20 meV [8]. (e) Δ_{CF} with variations of θ for R[100] and R[110] KO_2. Δ_{CF} increases monotonically with θ. (f) Δ_{KK} vs θ for R[110] KO_2. Δ_{KK} can be obtained by the total-energy difference between the AFM and FM states per formula unit, which corresponds to $4J_{eff}$. Here, J_{eff} is the effective interplane superexchange interaction between two superoxide ions. The DFT + U + SOC calculations with various U values were employed. (g) Δ_{CF}-$|\Delta_{KK}|$ vs θ for R[110] KO_2. KK inside the figure represents the KK-type quantum superexchange interaction dominant regime, while CF represents the classical CF dominant regime.

To obtain T-dependent electronic structures of strongly correlated $2p$ electrons in KO_2, we performed the DMFT calculations [28]. We have considered only the partially filled π_g^* orbitals for the DMFT calculation. The total bandwidth (W) of π_g^* orbital is obtained to be ~1 eV from the DFT calculation. We have determined the noninteracting part of the Hamiltonian using the downfolding scheme of Kohn-Sham DFT orbitals in the maximally localized Wannier function (MLWF) basis [29]. The interacting part of the Hamiltonian is given by

$$H_I = U \sum_{m,\mathbf{R}} n_{m,\mathbf{R},\uparrow} n_{m,\mathbf{R},\downarrow} + U' \sum_{m>l,\mathbf{R},\sigma} n_{m,\mathbf{R},\sigma} n_{l,\mathbf{R},\bar{\sigma}} + (U' - J) \sum_{m>l,\mathbf{R},\sigma} n_{m,\mathbf{R},\sigma} n_{l,\mathbf{R},\sigma}, \quad (1)$$

where U, U', and J are the intra-, interorbital Coulomb correlation, and the Hund interaction parameters, respectively. $n_{m,\mathbf{R},\sigma}$ represents the occupation number at orbital m, site R, and spin σ. We considered here the rotationally symmetric interaction, so that $U' = U - 2J$. We used interaction parameters of $U = 3.55$ eV and $J = 0.62$ eV, which were obtained by a constrained local-density approximation and random-phase approximation [8]. Thus, in view of $U/W > 1$, KO_2 is in the Mott insulator regime, as will be discussed further. We used the continuous time quantum Monte-Carlo (CTQMC) method as an impurity solver [30,31].

As shown in Fig. 1(d), the orbital degeneracy of the π_g^* level in KO_2 is to be lifted either (i) by the CF due to coherent rotation of superoxide ions, (ii) by the quantum superexchange interaction of the KK type, or (iii) by the intrasite SOC. The CF acts like a JT effect to make the π_y orbital have higher energy than the π_x orbital with the energy gap of Δ_{CF}. The KK-type superexchange would lift the degeneracy of the π_g^* level with preference of electron delocalization along the orbital order by the energy gap of Δ_{KK}. The intrasite SOC would split the degenerate π_g^* level into $\pi_{m=1}$ and $\pi_{m=-1}$ orbitals with an energy gap of Δ_{SO} (~20 meV) [8,10]. In reality, the relative magnitude of Δ_{CF}, Δ_{KK}, and Δ_{SO} would determine the splitting mechanism of the π_g^* level in KO_2. Then, the partially filled π_H orbitals are split further by the Coulomb repulsion to exhibit the Mott-Hubbard gap (Δ_{MH}). Δ_{MH} corresponds to the band gap of the electronic structure. Using the DFT + U + SOC, we have obtained that Δ_{MH} is between 0.24 and 1.20 eV, confirming the Mott insulating state of KO_2. This Mott insulating state is consistent with our DMFT result below.

Let us compare the relative magnitude of Δ_{CF} and Δ_{KK}, for R[110] KO_2. Figure 1(e) presents Δ_{CF} as a function of rotation angle θ, which is obtained by the on-site noninteracting part of the Hamiltonian in the MLWF basis. Δ_{CF} increases monotonically with θ for both rotations around the [100] and [110] axes, implying that the JT-type CF generates the π_y-hole FO ordering at low T. Note that Δ_{KK} corresponds to the superexchange energy gain per superoxide ion, which can be estimated by the total-energy difference ($4J_{eff}$) between the AFM and ferromagnetic (FM) states of R[110] KO_2 assuming π_y-hole FO order [32]. Here, J_{eff} represents the effective interplane superexchange interaction strength between two superoxide ions. Figure 1(f) shows Δ_{KK} as a function of θ, which shows that the AFM phase becomes more stable for $\theta > 5^\circ$ in R[110] KO_2.

In Fig. 1(g), we compare the Δ_{CF} and $|\Delta_{KK}|$ values as a function of θ for R[110] KO_2. For $\theta < 10^\circ$, $\Delta_{CF} - |\Delta_{KK}|$ is negative, which implies that the KK-type quantum superexchange effect dominates over the CF effect. In this regime, Δ_{SO} has a comparable magnitude to Δ_{KK} (~20 meV). As a result, the orbital ordering in this regime is driven by the competing superexchange interaction and SOC. In contrast, for $\theta > 10^\circ$, $\Delta_{CF} - |\Delta_{KK}|$ becomes positive, which implies that the classical JT-type CF is dominating. In this regime, Δ_{CF} is larger than Δ_{SO}. As a result, the orbital ordering is driven solely by the CF. At $\theta = 10^\circ$, the $\Delta_{CF} - |\Delta_{KK}|$ value is close to zero, which indicates the competition of two mechanisms.

We have performed the DMFT calculations to obtain finite-T electronic structures of KO_2 for different crystal structures. Figure 2 presents the imaginary parts of Green's functions and self-energies for π_x and π_y orbitals of KO_2 at room temperature ($T = 300$ K). The imaginary part of the Green's function for each structure has zero value and negative derivative at $\omega_n = 0$ (ω_n: Matsubara frequency), implying that KO_2 is an insulator at room temperature. The imaginary parts of self-energies for the

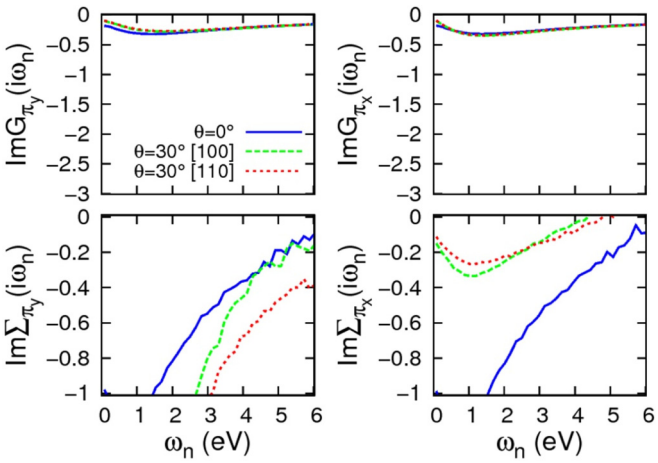

FIG. 2. (Color online) DMFT results for the imaginary part of the Green's functions $G(i\omega_n)$ and self-energies $\Sigma(i\omega_n)$ for the π_x and π_y orbital at $T = 300$ K. Blue (solid), green (dashed), and red (dotted) lines are for $\theta = 0^\circ, \theta = 30^\circ$ around [100], and $\theta = 30^\circ$ around [110] structures of KO_2, respectively.

π_x and π_y orbitals have similar values for $\theta = 0^\circ$. In contrast, the imaginary part of self-energy for the π_y orbital is much larger than that of π_x near $\omega_n = 0$ for $\theta = 30^\circ$ of both the R[100] and R[110] structures. This behavior of self-energies suggests that there exists an orbital fluctuation at $\theta = 0^\circ$, but this orbital fluctuation is suppressed with the emergence of π_y-hole FO ordering for $\theta = 30^\circ$ structures. This feature will be seen more clearly in Fig. 3 below.

On the basis of the DMFT results, we have obtained the orbital state phase diagram with respect to T and the crystal structure of KO_2. Figure 3 presents T-dependent orbital polarization for each rotated structure. We define the orbital polarization as $P = (P_{\pi_y} - P_{\pi_x})/(P_{\pi_y} + P_{\pi_x})$, where

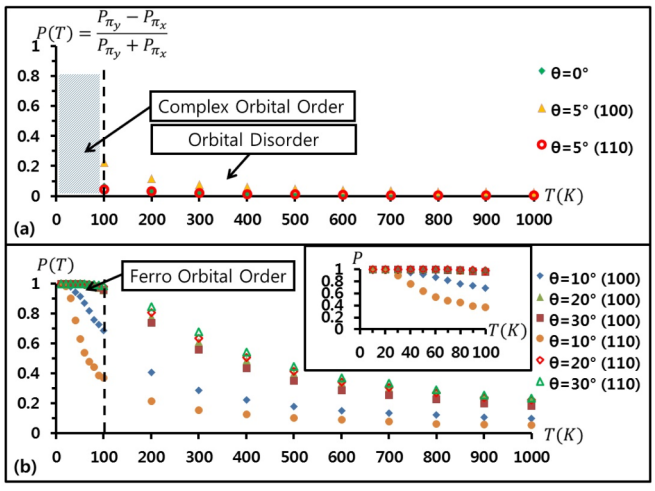

FIG. 3. (Color online) (a) DMFT results for orbital polarization (P) of KO_2 vs temperature (T) for small rotations ($\theta = 0^\circ$ and 5°). The regimes of orbital disorder and complex orbital order are indicated. (b) The same as (a) for large rotations ($\theta = 10^\circ$, 20°, and 30°). The π_y-hole FO state with full orbital polarization is achieved below 100 K. Inset provides P vs T for $T < 100$ K.

P_{π_a} indicates the probability of a π_a-hole orbital state in the DMFT calculation. For small rotation ($\theta \leqslant 5^\circ$) in Fig. 3(a), the orbital polarization P is close to zero for $T > 100$ K, which indicates that the orbital state of KO_2 is disordered at high T. This feature is consistent with the orbital fluctuation feature, as discussed in Fig. 2 for $\theta = 0^\circ$. With lowering T below 100 K, we observed the irregular oscillation between P_{π_x} and P_{π_y} during iterations of the self-consistency loop, which reveals the complex orbital state in this regime. One possible candidate state in this regime would be the antiferro-orbital (AFO) ordering state, as suggested for RbO_2 and CsO_2 [15], in which θ are smaller than 5° [14,18]. As discussed in Fig. 1(g), for small θ, the KK-type superexchange effect dominates over the CF effect. The signature of AFO ordering in this regime indicates that the orbital order is driven by the quantum superexchange interaction rather than the classical CF. In other words, the absence of the FO ordering in RbO_2 and CsO_2 can be understood in terms of their small rotation angles, which do not produce strong enough CF to generate the FO ordering.

For large rotation angles ($\theta > 10^\circ$) in Fig. 3(b), the full orbital polarization is achieved around 100 K with the suppression of the orbital fluctuation. This result indicates that, in KO_2, the AFM spin ordering at low T is realized with the emergence of FO ordering. At large θ, the CF effect dominates over the superexchange effect, whereby the π_y-hole FO ordering emerges in the large rotation structures. At $\theta = 10^\circ$, these two mechanisms compete. As a result, it is seen in Fig. 3(b) that the π_y-hole FO ordering occurs only at very low T of ~20K.

Notice that the orbital fluctuation in the rare-earth vanadates, such as $LaVO_3$, was characterized by the glassy behavior of thermal conductivity [1,4,33]. In $LaVO_3$, the thermal conductivity becomes much reduced due to scattering of phonons by disordered orbital states. According to the phase diagram in Fig. 3(a), such orbital fluctuation exists in KO_2 at room-temperature T. Then we expect the suppression of thermal conductivity in KO_2 due to this orbital fluctuation. The comparison of the thermal conductivities between KO_2 and peroxide BaO_2 that has fully occupied π_g^* orbitals would give great insight into the orbital fluctuation effect in KO_2 [34]. Further, if the orbital fluctuation is suppressed upon cooling, the thermal conductivity of KO_2 would be recovered from the glassy behavior to become close to that of BaO_2. In fact, the suppression of orbital fluctuation with rotation of O_2^- anion axes was recently observed in Cs_4O_6, which has mixed valences of closed-shell peroxide O_2^{2-} and open-shell superoxide O_2^- anions [35].

To examine the possible orbital state for small θ and to confirm that the π_y-hole FO order is compatible with the observed AFM structure for large θ, we have performed total-energy calculations in the DFT + U + SOC for various orbital states. We have obtained at $\theta = 0^\circ$ that KO_2 has the stable $(x + y, x - y)$-hole AFO ordering state (see Fig. S2 in the Supplemental Material [32]). Here, the (a,b)-hole state represents the π_a and π_b-hole orbital states for two superoxide ions in the $(1 \times 1 \times 1)$ tetragonal unit cell [32]. Directional coordinates for (a,b) are depicted in Fig. 1. Noteworthy is that the SOC is known to play an important role in the ground state of KO_2 at $\theta = 0^\circ$ [8,10]. Δ_{SO} in KO_2 is as much as ~20 meV [8], and the large orbital moment was

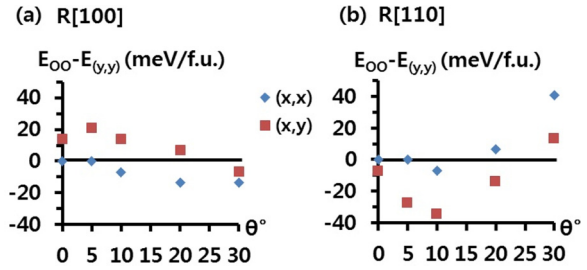

FIG. 4. (Color online) (a) Total-energy differences between different orbital ordering (OO) states vs θ for R[100] KO_2. Experimental AFM structure has been assumed. We used the DFT + U + SOC method with $U = 4$ eV. Results are consistent for U values of 4–10 eV. We set the (y,y) state as the zero-energy state. (b) The same as (a) for R[110] KO_2.

indeed observed in isolated superoxides [36]. As mentioned earlier, Δ_{SO} and Δ_{KK} have comparable magnitude at $\theta = 0^\circ$, suggesting the competition between the superexchange-driven AFO order and the SOC-driven π_g^* level splitting. Actually, we have confirmed that the SOC-induced state with azimuthally symmetric hole orbital shape has a comparable total energy to the $(x + y,x - y)$-hole state [32,37].

This result for $\theta = 0^\circ$ corroborates our earlier finding that the FO order will not be realized in superoxides having small rotation angle θ. RbO_2 and CsO_2 have $\theta \approx 0^\circ$. For RbO_2, the emergence of in-plane AFO ordering with cation distortions was reported [11,13,14]. For CsO_2, there was a report that the high-T phase exhibits the Curie-Weiss magnetic susceptibility with large orbital moment contribution, while the low-T phase exhibits the in-plane AFO order with superexchange interaction and cation distortion [14]. Therefore, distinct from KO_2 which has the dominant CF effect, RbO_2 and CsO_2 have the interplay between various interaction effects including the KK-type superexchange, the SOC, and the cation distortion.

As shown in Fig. 4, for the given experimental AFM structure of KO_2, only the R[110] structure has the stable π_y-hole FO (y,y) state at finite $\theta \sim 30^\circ$, as is consistent with the DMFT result of Fig. 3(b). In contrast, the R[100] structure in Fig. 4(a) does not favor the π_y-hole FO state at $\theta \sim 30^\circ$ because the FO (y,y) state tends to induce the AFM interaction along the [010] direction that is not compatible with the experimental AFM structure. This result is consistent with that of Ref. [10] and the observed phase diagram at low T. It thus suggests that the structural transition from R[100] with $\theta = 20^\circ$ to R[110] with $\theta = 30^\circ$ at 10 K occurs through the strong connection between the FO ordering and the AFM transition.

In conclusion, we have investigated T-dependent orbital states and magnetism of KO_2 based on the DFT and DMFT calculations. At high T, KO_2 exhibits the orbital fluctuation. Upon cooling, the FO state emerges with the large coherent rotation of superoxide ions and the corresponding enhancement of the JT-type CF. This FO state is compatible with the observed AFM spin ordering at low T only for the rotation around the [110] axis. In RbO_2 and CsO_2, the rotation angle is inherently too small to generate the FO ordering. Instead, in RbO_2 and CsO_2, the AFO ordering occurs through the interplay between various interaction effects including the KK-type superexchange, the SOC, and cation distortion. The suppression of the orbital fluctuation at room temperature can be probed from the comparative measurements of thermal conductivities for KO_2 and BaO_2.

This work was supported by the NRF (Grant No. 2009-0079947) and by the KISTI supercomputing center (Grant No. KSC-2012-C3-056).

[1] G. Khaliullin, Prog. Theor. Phys. Suppl. **160**, 155 (2005).
[2] G. Khaliullin, P. Horsch, and A. M. Oleś, Phys. Rev. Lett. **86**, 3879 (2001).
[3] M. De Raychaudhury, E. Pavarini, and O. K. Andersen, Phys. Rev. Lett. **99**, 126402 (2007).
[4] J.-S. Zhou, Y. Ren, J.-Q. Yan, J. F. Mitchell, and J. B. Goodenough, Phys. Rev. Lett. **100**, 046401 (2008).
[5] P. Horsch, A. M. Oleś, L. F. Feiner, and G. Khaliullin, Phys. Rev. Lett. **100**, 167205 (2008).
[6] E. Pavarini, E. Koch, and A. I. Lichtenstein, Phys. Rev. Lett. **101**, 266405 (2008).
[7] E. Pavarini and E. Koch, Phys. Rev. Lett. **104**, 086402 (2010).
[8] I. V. Solovyev, New J. Phys. **10**, 013035 (2008).
[9] R. Kováčik and C. Ederer, Phys. Rev. B **80**, 140411(R) (2009).
[10] M. Kim, B. H. Kim, H. C. Choi, and B. I. Min, Phys. Rev. B **81**, 100409(R) (2010).
[11] E. R. Ylvisaker, R. R. P. Singh, and W. E. Pickett, Phys. Rev. B **81**, 180405(R) (2010).
[12] A. K. Nandy, P. Mahadevan, P. Sen, and D. D. Sarma, Phys. Rev. Lett. **105**, 056403 (2010).
[13] K. Wohlfeld, M. Daghofer, and A. M. Oleś, Europhys. Lett. **96**, 27001 (2011).
[14] S. Riyadi, B. Zhang, R. A. de Groot, A. Caretta, P. H. M. van Loosdrecht, T. T. M. Palstra, and G. R. Blake, Phys. Rev. Lett. **108**, 217206 (2012).
[15] R. Kováčik, P. Werner, K. Dymkowski, and C. Ederer, Phys. Rev. B **86**, 075130 (2012).
[16] I. V. Solovyev, Z. V. Pchelkina, and V. V. Mazurenko, Cryst. Eng. Comm. **16**, 522 (2014).
[17] M. Kim and B. I. Min, Phys. Rev. B **84**, 073106 (2011).
[18] M. Labhart, D. Raoux, W. Känzig, and M. A. Bösch, Phys. Rev. B **20**, 53 (1979).
[19] W. Känzig and M. Labhart, J. Phys. (Paris) **37**, C7 (1976).
[20] There were theoretical predictions for the zero-T crystal structure of KO_2 [12,21,22], which are different from that of Fig. 1(c). In fact, the predicted crystal structures are different between Ref. [12] and Refs. [21,22], even though these reports were from the same group. This inconsistency indicates that more elaborate theoretical studies on the crystal structure of KO_2 are demanded.
[21] A. K. Nandy, P. Mahadevan, and D. D. Sarma, Phys. Rev. B **84**, 035116 (2011).

[22] A. K. Nandy, P. Mahadevan, and D. D. Sarma, Mol. Sim. **38**, 1308 (2012).
[23] H. G. Smith, R. M. Nicklow, L. J. Raubenheimer, and M. K. Wilkinson, J. Appl. Phys. **37**, 1047 (1966).
[24] M. Weinert, E. Wimmer, and A. J. Freeman, Phys. Rev. B **26**, 4571 (1982).
[25] P. Blaha, K. Schwarz, G. K. H. Madsen, D. Kavasnicka, and J. Luitz, computer code WIEN2k (Karlheinz Schwarz, Technische Universitat Wien, Austria, 2001).
[26] V. I. Anisimov, I. V. Solovyev, M. A. Korotin, M. T. Czyżyk, and G. A. Sawatzky, Phys. Rev. B **48**, 16929 (1993).
[27] The convergence of the total-energy difference between different electronic structures was checked down to 7 meV per formula unit.
[28] G. Kotliar, S. Y. Savrasov, K. Haule, V. S. Oudovenko, O. Parcollet, and C. A. Marianetti, Rev. Mod. Phys. **78**, 865 (2006).
[29] A. A. Mostofi, J. R. Yates, Y.-S. Lee, I. Souza, D. Vanderbilt, and N. Marzari, Comp. Phys. Comm. **178**, 685 (2008).
[30] K. Haule, Phys. Rev. B **75**, 155113 (2007).
[31] P. Werner, A. Comanac, L. de' Medici, M. Troyer, and A. J. Millis, Phys. Rev. Lett. **97**, 076405 (2006).
[32] See Supplemental Material at http://link.aps.org/supplemental/10.1103/PhysRevB.89.121106 for various magnetic and orbital orderings, and the total-energy differences between them.
[33] J.-Q. Yan, J.-S. Zhou, and J. B. Goodenough, Phys. Rev. Lett. **93**, 235901 (2004).
[34] W. Wong-Ng and R. S. Roth, Physica C **233**, 97 (1994).
[35] D. Arčon, K. Anderle, M. Klanjšek, A. Sans, C. Mühle, P. Adler, W. Schnelle, M. Jansen, and C. Felser, Phys. Rev. B **88**, 224409 (2013).
[36] P. D. C. Dietzel, R. K. Kremer, and M. Jansen, J. Am. Chem. Soc. **126**, 4689 (2004).
[37] We have confirmed that the SOC-induced state with spin direction along [001] has a comparable energy to the $(x + y, x - y)$-hole state. In the electron paramagnetic resonance (EPR) experiment at $T < 200$ K, the spin direction was found to be normal to the molecular direction [18].